ROLE OF JOULE HEATING ON THE HYDRODYNAMIC BOUNDARY LAYER WITH RECTANGULAR ELECTRODES – NUMERICAL APPROACH

M. A. OYANADER† and P. E. ARCE‡

† *Dpto. de Ing. Quimica, Univ. Católica del Norte, Angamos 0610, Antofagasta, Chile. MOyanader@tntech.edu*
‡ *Chemical Engng. Department, Tennessee Tech. University, Prescott Hall 214, Cookeville, TN 38505-USA. PArce@tntech.edu*

***Abstract*— This contribution focuses on the analysis of the role of Joule heating on the hydrodynamics of systems where buoyancy is an important driving force. Typical examples are electrokinetic applications for soil cleaning and macromolecules separation. In particular, the region of interest for this study is the zone near vertical-rectangular electrodes. The analysis is conducted for boundary layer flows due to natural convection as a result of heat generation caused by the applied electrical field. A numerical solution of the differential model equations yields the temperature profile, the boundary layer thickness, and the component of the velocity field along the axial and transversal directions of the electrode. Effects of the heat generation on temperature, velocity profiles and boundary layer thickness are simulated and discussed. The results of the analysis allow a better assessment of the role of Joule heating on the hydrodynamics of the system near the electrode.**

***Keywords*— Hydrodynamics, Joule heating, Boundary Layer, Numerical Solution, Modeling Approach.**

I. INTRODUCTION AND MOTIVATION

Joule heat generation, due to the electrical resistivity of the media, is a common feature of many processes when an applied electrical field is present. Examples of these applications includes electrokinetic soil remediation and electrophoretic separation. These promising technologies are in need of more understanding of the different fundamental flows and driving forces controlling the process during operation (Acar *et al.*, 1995; Masliyah, 1994). Different arrangements, of the same technology, tend to favor different and specific mechanisms that usually drive the mass transfer and/or the hydrodynamics of the system. Moreover, the intrinsic complexity of the associated transport mechanisms in these applications inhibits the scaling of conceptual designs to field practices (Virkutyte et al., 2002; Ho et al. 2002). Therefore, in this contribution we focus on the analysis of the effect of Joule heating generation on the flow situation found in the hydrodynamic boundary layer near the electrode region. For example, in an electrokinetic cell there are two main regions of interest; they are the treatment zone and the electrodes zone (Oyanader, 2004). The treatment region has received some attention (Oyanader *et al.*, 2003; Oyanader, 2004; Oyanader *et al.*, 2005a, Oyanader *et al.*, 2005b) but the region near electrodes is less studied in the literature. This last one becomes the focus of attention in technological applications where the location of the chemical reaction and/or the point of fluid extraction are near the electrodes. Electrokinetic remediation methodologies, in which this particular zone is a key for technology success, are for example cation selective membrane, ceramic casting, electrochemical ion exchange and specific cases of Lasagna process (Acar *et al.*, 1995). As a consequence, knowing the hydrodynamics of the system in such an important region is highly desired. Furthermore, it is useful to know the relative effect of the transport mechanisms that come into play when greater differential potentials are applied. Among these mechanisms are: the convective and buoyancy forces not yet fully studied in the literature.

In general, misconceptions about the ability of electrical based field applications in yielding good results under particular field conditions are the consequences of little fundamental research on the engineering science part of systems. Several variables are reported as controlling removal or separation efficiency. To some researchers, water content as well as pH is believed to be responsible for process efficiency (Virkutyte *et al.*, 2002; Yeung *et al*., 1997). In particular, this is the case of ceramic casting where, in a controlled volume of contaminated soil, buffer solution is added to ensure a constant value of water content and pH. However, there is another important controlling variable; this is the Joule heating effect which is equally responsible for affecting removal efficiency, although not necessarily well understood (Oyanader *et al.*, 2003; Oyanader, 2004; Oyanader *et al.*, 2005a; Oyanader *et al.*, 2005b; Yeung *et al*., 1997, Erdmann *et al.*, 2005).

Currently in the literature, there is a lack of agreement as to how the Joule heating phenomenon would affect the process behavior. For example, several authors have reported the development of high temperature on electrokinetic processes of soil remediation during operation. One of them, further reports that the electroosmotic mechanism seems to be affected when temperature rises and as a result low process efficiency is obtained (Yeung *et al.*, 1997). Conversely, increase of temperature is reported to be beneficial to the fluiddynamics of hydrocarbons-containing fluids in that their

viscosity is reduced (Chilingar *et al.*, 1997). To introduce even more conflicting ideas, overheating is recognized as an operational phenomenon that has to be avoided (Ho *et al.*, 1997; Chilingar *et al.*, 1997; Langeman, 1993). And finally, it has been concluded that one of the disadvantages of electrokinetic remediation is that the increase of temperature decreases the efficiency of the process (Virkutyte *et al.*, 2002). Therefore, it is important to explain, the role of temperature (and its relation to Joule heating) on the hydrodynamic flows inside the boundary layer near the electrode region. This would allow practitioners to: 1) understanding the process behavior, 2) achieving new technological development, 3) identifying optimal operating condition, and, perhaps, 4) identifying cost efficient processes. In consequence, this investigation will focus on specialized cases of boundary layer flows, with low Reynolds number, in vertical and rectangular electrodes. Furthermore, a numerical scheme has been used to solve the final differential equation modeling the boundary layer thickness and velocity profiles.

II. MODEL FORMULATION

For the region near rectangular electrodes, the hydrodynamic problem described above suggests that the best modeling approach is a boundary layer analysis. Turnbull (1969) discussed the effects of an electric field across the flow of a fluid but neglected any form of heat generation (source term). The addition of the Joule heating generation term leads to a *unique* situation where the coupling between energy and momentum equations needs careful attention. The differential model resulting from these equations will be studied with the Von Karman boundary layer approximation to obtain a two-ordinary differential equation model that will be solved numerically with appropriate boundary conditions. The methodology is particularly useful to investigate the flow problem and find important information about the hydrodynamic behavior near the electrode surface. In the section below, the geometry and schematic of the system are described and the model equation formulated.

A. System Description

The system represented in Fig. 1 is a two-dimensional system since no variation in the z-direction has been assumed. The vertical axis of the device coincides with the x-direction while the y-direction is horizontal. A vertical plate with a temperature T_0 is placed in a fluid with a temperature T_∞ which remains as the temperature of the fluid away from the plate during the analysis. Because of the differences in the temperature T_0 and T_∞, there are changes in velocity and they are confined to a thin boundary layer at the immersed plate. These changes are caused by the variation in the density of the fluid, which is caused by the temperature difference between the wall and the fluid. Thus, there is a motion caused by free convection within the boundary layer adjacent to the vertical wall. A voltage difference is assumed and applied across the fluid creating a uniform electric field in the y-direction. This type of electric field provides, for example, a driving force that causes electrophoresis to occur at a given rate and in a cell or the electro-mechanism in an electrokinetic remediation. A heat source, Q, is located within this layer due to the Joule heating effect caused by the electro-resistivity of the media. This heat generation could modify the temperature differences inside the boundary layer of the fluid near the vertical wall and, therefore, could influence the driving force for the hydrodynamics of the system. The heat source, Q, is maintained at a uniform value inside the boundary layer thickness. The equations for the mathematical boundary layer model will be derived and their assumptions, discussed in the sections below. In particular, this task will be performed in the sections 2.A and 2.B.

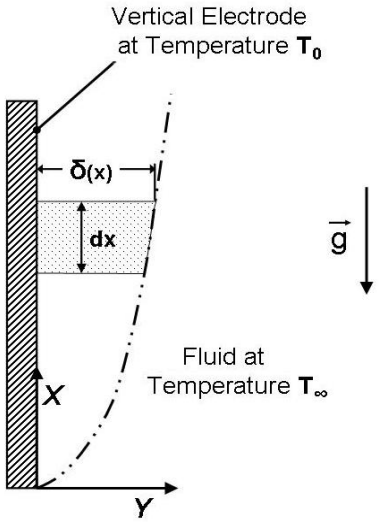

Figure 1: Sketch of a control volume and main variables associated with the boundary layer flow in a flat electrode geometry used in the analysis.

B. Equations of Energy and Motion

In terms of the energy conservation, Squire (1938) and Turnbull (1969) assumed that the velocity of the fluid and the current carried by the fluid were small enough so that the heat they generate was considered negligible. In the present article, this assumption will be relaxed to include the heat generation term in the conservation of energy equation (Bird *et al.*, 1960), this is

$$\rho \cdot C_p \frac{DT}{Dt} = \nabla \bullet (k \cdot \nabla T) + Q, \qquad (1)$$

where D is used to indicate the Lagrangian derivative, ρ the fluid density, C_p the specific heat, and k the thermal conductivity of the fluid.

Using dimensionless variables, *i.e.* transforming from *x,y* coordinate system to a dimensionless ξ, η system, the following single expressions are introduced:

Characteristic Length[1]

[1] The choice of the characteristic parameters is motivated by the relevant literature on buoyancy driven flows. (Gebhart *et al.* , 1988)

$$L = \left[\frac{\mu^2}{\rho_0^2 \cdot g \cdot \beta \cdot (T_0 - T_\infty)} \right]^{1/3} . \quad (2)$$

Thermal Velocity

$$v_T = \frac{k}{\rho \cdot C_p} \frac{1}{L} = \alpha \frac{1}{L} . \quad (3)$$

where μ is the fluid viscosity, β the coefficient of volume expansion (Bird *et al.*, 1960) and α the thermal diffusivity. By using the parameters identified previously and assuming steady-state conditions, the following non-dimensional differential equation is obtained for energy

$$v_x^+ \cdot \frac{\partial \theta}{\partial \xi} + v_y^+ \cdot \frac{\partial \theta}{\partial \eta} = \frac{\partial^2 \theta}{\partial \eta^2} + \phi^2 . \quad (4)$$

This form of the energy equation is obtained under the steady-state boundary layer approximation and the fact that conduction is assumed important only in the transversal direction for the system shown in Fig. 1. The following additional definition of dimensionless variables applies

$$v_x^+ = \frac{v_x}{v_T}; \quad v_y^+ = \frac{v_y}{v_T};$$

$$\theta = \frac{T - T_\infty}{T_0 - T_\infty}; \phi^2 \equiv \frac{Q \cdot L^2}{k \cdot (T_0 - T_\infty)} \quad (5)$$

$$\xi = \frac{x}{L}; \qquad \eta = \frac{y}{L} . \quad (6)$$

Further simplification of the problem assumes that all physical properties of the fluid, except for density, are independent of temperature. In addition, the density will be assumed constant except in the gravitational term which is the usual Boussinesq approximation (Whitaker, 1991). Furthermore, the continuity equation is given by the usual form for incompressible flow situation (Whitaker, 1991; Bird *et al.*, 1960), thus, $\nabla \bullet v = 0$, written for the planar geometry reduces to:

$$\frac{\partial v_x}{\partial x} + \frac{\partial v_y}{\partial y} = 0 \quad (7a)$$

$$\frac{\partial v_x^+}{\partial \xi} + \frac{\partial v_y^+}{\partial \eta} = 0 \text{ (Dimensionless)} \quad (7b)$$

for the case of incompressible flow.

The Navier-Stokes equation (Whitaker, 1991) will be assumed applicable since only Newtonian fluids will be considered in the analysis, this is

$$\rho \frac{Dv}{Dt} = -\nabla p + \mu \cdot \nabla^2 v + \rho \cdot g , \quad (8a)$$

where the gravity is assumed constant and it is indicated by g, p is used to denote the pressure, and μ, the fluid viscosity. For this analysis, it is assumed that the electrical field does not affect the hydrodynamic field. The density ρ, as a function of temperature, is given by (Bird *et al.*, 1960)

$$\rho = \rho_0 \cdot [1 - \beta \cdot (T - T_\infty)] , \quad (8b)$$

where ρ_0 is the density at a given reference temperature for the system and β is the same as defined after Eq. 3.

Based on the discussion given in section one above, the variation in temperature is confined to the boundary layer adjacent to the surface wall, for example, of the electrode of an electrokinetic remediation cell. This situation occurs, when the temperature and velocity profiles in a system show appreciable gradients across the system in the neighborhood of the surface. Under these conditions, energy, and momentum transport equations can be applied in the "boundary layer" near the wall domain. Therefore, the usual boundary layer approximations will be made in the momentum, energy, and continuity equations to build the differential mathematical models. In order to obtain the boundary layer equations, they are formally integrated with respect to "y" across the boundary layer thickness, δ. Momentum and energy boundary layer thicknesses are assumed to be equal. For cases without generation, this assumption works well when the Prandtl number is equal to one (Whitaker, 1991).The final result (after the integration is performed) yields two first-order differential equations. In the section below, the mathematical boundary layer model associated with the system under study is derived. For such a purpose, components of the Navier-Stokers equations (Bird *et al.*, 1960) in the x and y directions of the system are written for a Cartesian system of coordinates as

Coordinate x:

$$\rho_0 \cdot \left(v_x \cdot \frac{\partial v_x}{\partial \xi} + v_y \cdot \frac{\partial v_x}{\partial \eta} \right) =$$

$$-\frac{\partial p}{\partial x} - g \cdot \rho_0 \cdot [1 - \beta \cdot (T - T_\infty)] + \mu \cdot \left(\frac{\partial^2 v_x}{\partial \xi^2} + \frac{\partial^2 v_x}{\partial \eta^2} \right) \quad (9a)$$

$$v_x^+ \cdot \frac{\partial v_x^+}{\partial \xi} + v_y^+ \cdot \frac{\partial v_x^+}{\partial \eta} = \frac{1}{Re} \left(\frac{\partial^2 v_x^+}{\partial \xi^2} + \frac{\partial^2 v_x^+}{\partial \eta^2} \right) + \frac{Gr}{Re^2} \theta \cdot$$

(Dimensionless) (9b)

Coordinate y:

$$\rho_0 \cdot \left(v_x \cdot \frac{\partial v_y}{\partial \xi} + v_y \cdot \frac{\partial v_y}{\partial \eta} \right) = +\mu \cdot \left(\frac{\partial^2 v_y}{\partial \xi^2} + \frac{\partial^2 v_y}{\partial \eta^2} \right) \quad (10a)$$

$$v_x^+ \cdot \frac{\partial v_y^+}{\partial \xi} + v_y^+ \cdot \frac{\partial v_y^+}{\partial \eta} = \frac{1}{Re} \left(\frac{\partial^2 v_y^+}{\partial \xi^2} + \frac{\partial^2 v_y^+}{\partial \eta^2} \right)$$

(Dimensionless) (10b)

where the following definition of dimensionless numbers applies

$$Re = \frac{\rho_0 \cdot v_T \cdot L}{\mu}; \quad Gr = \frac{\rho_0^2 \cdot g \cdot \beta \cdot (T_0 - T_\infty) \cdot L^3}{\mu^2} . \quad (11)$$

Equation 9 (a-b) show the driving force term given by Eq. 8, *i.e.*, the free-convective term, caused by the tem-

perature difference between the vertical wall and the fluid.

Note that axial component contains the density variation because the coordinate "x" is in the vertical direction of the system. As previously mentioned the motion of the fluid is only two-dimensional, hence the z-component of the momentum equation is irrelevant.

By applying the methodology described above, to Eqs. 9b and 10b with the modifications herein proposed, the differential equations for boundary layer approximations will be derived for the energy and momentum equations. Therefore, the partial derivative of Eqs. 9b and 10b, with respect to orthogonal coordinates, can be combined and reduced using Eq. 7b to yield

$$v_x^+ \cdot \left(\frac{\partial^2 v_y^+}{\partial \xi^2} + \frac{\partial^2 v_y^+}{\partial \eta^2} \right) - v_y^+ \cdot \left(\frac{\partial^2 v_x^+}{\partial \xi^2} + \frac{\partial^2 v_x^+}{\partial \eta^2} \right) =$$

$$\frac{1}{Re} \left(\frac{\partial^3 v_y^+}{\partial \xi^3} + \frac{\partial^3 v_y^+}{\partial \xi \partial \eta^2} - \frac{\partial^3 v_x^+}{\partial \xi^2 \partial \eta} - \frac{\partial^3 v_x^+}{\partial \eta^3} \right) - \frac{Gr}{Re^2} \theta \,. \quad (12)$$

Equation 12 can be simplified further if the order of magnitude of the derivative with respect to transversal coordinate is assumed to be much larger than the one of the derivative with respect to axial (Whitaker, 1991), *i.e.*

$$\frac{\partial(\bullet)}{\partial \eta} >> \frac{\partial(\bullet)}{\partial \xi} \quad (13)$$

This assumption is justified since the width of the boundary layer, δ, is much smaller than any characteristic dimension in the x-direction. In addition, the magnitude of the velocity component, v_x, is considered to be much larger than the one of the other velocity component, v_y. Next, by combining Eqs. (12) and (13), the following equation can be written

$$v_x^+ \cdot \frac{\partial^2 v_y^+}{\partial \eta^2} - v_y^+ \cdot \frac{\partial^2 v_x^+}{\partial \eta^2} = -\frac{1}{Re} \frac{\partial^3 v_x^+}{\partial \eta^3} - \frac{Gr}{Re^2} \theta \,. \quad (14)$$

Now, by integrating Eq. 14 with respect to the transversal coordinate (some terms by parts), and by using Eq. 7b, the following equation is derived

$$v_x^+ \cdot \frac{\partial v_x^+}{\partial \xi} + v_y \cdot \frac{\partial v_x^+}{\partial \eta} = \frac{1}{Re} \frac{\partial^2 v_x^+}{\partial \eta^2} + \frac{Gr}{Re^2} \theta - C(\xi) \quad (15)$$

where C(ξ) is an integration constant. In order to compute C(ξ), the boundary condition used is located at the surface wall of the electrode. At this position, the magnitude of the velocity profile is zero and the temperature of the fluid is uniform and given by T_0. Therefore,

$$C(\xi) = \frac{Gr}{Re^2} \cdot \quad (16)$$

Equation (16) shows that actually C(ξ) is independent of the axial coordinate. Finally, the momentum equation for the boundary layer with free convection terms is given by

$$v_x^+ \cdot \frac{\partial v_x^+}{\partial \xi} + v_y^+ \cdot \frac{\partial v_x^+}{\partial \eta} = \frac{1}{Re} \frac{\partial^2 v_x^+}{\partial \eta^2} + \frac{Gr}{Re^2} (\theta - 1) \cdot \quad (17)$$

Equations (4) and (17) need boundary conditions to be solved. However, since the Von Karman integral approximation will be used in this approach, the analysis of the boundary conditions is delayed for a later stage of this article. The next step in the analyses of the system is to apply the Von Karman integral approximation to Eqs. (4) and (17) to invert the partial differential equation system, first, to an integro-differential model and, then into a two-equation ordinary differential model. This task is accomplished in the section below.

C. Derivation of Von Karman Integral Approximation

The integral approximation for boundary layer was originally developed by Von Karman (Whitaker, 1991). The method was subsequently used by Squire (1938) for the analysis of the buoyancy-driven boundary layer adjacent to a heated isothermal vertical surface. In order to apply such a methodology, Eqs. (4) and (17) are integrated over the transversal variable (y or η, see Fig. 1) from the plate (*i.e.*, y = 0, η=0) to the edge of the boundary layer, (*i.e.*, y = δ, η= δ^+). The conditions for the velocity and temperature fields involved in these integrals are

$$\begin{aligned} v_x^+ = v_y^+ = 0 \quad & \text{at} \quad \eta = 0, \delta^+ \\ \theta = 1 \quad & \text{at} \quad \eta = 0 \\ \theta = 0 \quad & \text{at} \quad \eta = \delta^+ \,. \end{aligned} \quad (18)$$

By integrating the equation of energy (4 above) and considering that ϕ^2 is constant in the transversal direction, across the boundary layer thickness, the following integro-differential equation may be derived

$$\frac{\partial}{\partial \xi} \int_0^{\delta^+} v_y^+ \cdot \theta \cdot \partial \eta = \int_0^{\delta^+} \frac{\partial^2 \theta}{\partial \eta^2} \cdot \partial \eta + \phi^2 \cdot \delta^+ \,. \quad (19)$$

By using the ideas of the integral approximation of the momentum equation, the integration of Eq. (17) above yields

$$\frac{\partial}{\partial \xi} \int_0^{\delta^+} \left(v_y^+ \right)^2 \cdot \partial \eta = \frac{1}{Re} \cdot \int_0^{\delta^+} \frac{\partial^2 v_x^+}{\partial \eta^2} \cdot \partial \eta + \frac{Gr}{Re^2} \cdot \int_0^{\delta^+} (\theta - 1) \cdot \partial \eta \quad (20)$$

which is the integral approximation for the energy-momentum equation with a uniform heat generation (due to the Joule effect) across the domain of the system.

The result of applying the Von Karman integral approximation is the two-equations model, Eqs. (19) and (20), that features the hydrodynamic velocity profile as well as the temperature profile inside the free- convection boundary layer at the electrode vertical wall. This model will be solved by the approach introduced by Squire (1938) and followed by Turnbull (1969). The methodology requires approximate expressions for the velocity profile, v_x^+, and for the temperature profile, θ, as functions of the variables. In the analysis by Turnbull, v_x^+ was obtained from a free convective based problem in the absence of an electric field. This ap-

proximation was initially proposed by Squire and it will be followed in this study. Therefore, the proposed dimensionless velocity profile is given by

$$v_x{}^+ = U^+ \cdot \frac{\eta}{\delta^+} \cdot \left(1 - \frac{\eta}{\delta^+}\right)^2, \qquad (21)$$

where U^+ is the dimensionless velocity amplitude in the ξ-direction (x-direction) and δ^+ the dimensionless boundary layer thickness, both obtained using the thermal velocity and characteristic length defined previously in section 2.B, above.

This particular form of velocity profile is used because, in the system under analysis, no fluid is entering the system since the driving force is provided by the temperature difference between the plate and the fluid.

For temperature the following profile will be used in this study to describe temperature variations in the boundary layer domain (Squire, 1938)

$$\theta = \left(1 - \frac{\eta}{\delta^+}\right)^2. \qquad (22)$$

Both, the velocity and temperature profiles are a function of the heat generation throughout the thickness of the boundary layer, δ. Also note that in both cases (*i.e.*, for the velocity and for the temperature profiles) a second-order polynomial is assumed. Moreover, U^+ and δ^+ are both functions of ξ (x non-dimensional) and are to be obtained from the governing integral-differential equations characteristic of this methodology (Turnbull, 1969). In consequence, after the proper substitution and integration is performed, the methodology yields the following two first-order differential equations

$$\frac{d}{d\xi}\left(\frac{1}{30} \cdot U^+ \cdot \delta^+\right) = \frac{2}{\delta^+} + \phi^2 \cdot \delta^+ \qquad (23)$$

$$\frac{d}{d\xi}\left(\frac{1}{105} \cdot U^{+2} \cdot \delta^+\right) = -\frac{2}{3} \cdot \frac{Gr}{Re^2} \cdot \delta^+ - \frac{1}{Re} \cdot \frac{U^+}{\delta^+}. \qquad (24)$$

These equations can be solved either numerically or analytically. The analytical solution has been developed the by authors using as boundary condition the region of the bulk fluid of the system. A comparison of results, between these two different approaches, has been partially documented elsewhere (see Oyanader, 2004). This work, however, concentrates on the numerical solution. Therefore, further algebraic development of Eqs. (23) and (24) yields the following differential system

$$\frac{dU^+}{d\xi} = -\left(\frac{105}{Re} + 60\right)\left(\frac{1}{\delta^{+2}}\right) - 70 \cdot \frac{Gr}{Re^2}\left(\frac{1}{U^+}\right) + 30 \cdot \phi^2 \qquad (25a)$$

$$\frac{d\delta^+}{d\xi} = \left(\frac{105}{Re} + 120\right)\left(\frac{1}{U^+ \cdot \delta^+}\right) + 70 \cdot \frac{Gr}{Re^2}\left(\frac{\delta^+}{U^{+2}}\right) - 60 \cdot \phi^2 \cdot \frac{\delta^+}{U^+} \qquad (25b)$$

$$\delta^+ = 0 \quad \text{at} \quad \xi = 0 \qquad (25c)$$

$$U^+ = 0 \quad \text{at} \quad \xi = 0 \qquad (25d)$$

This model system, represented by Eqs. (25a-d), is solved using conventional numerical methods. For simplicity reasons, the results reported in the next section were obtained using Euler method, some times called Heun's method (Kreyzing, 1999). The step size, required by the method, was selected very small in order to avoid inaccuracy and imprecision.

III. DISCUSSION AND ILLUSTRATIVE RESULTS

This section includes graphical illustrations for the solutions of the differential equations derived in section 2 of this paper. These illustrations are useful in gaining a deeper understanding of the system behavior and the role played by the Joule heating generation on the main variables of the system. Therefore, plots for boundary layer thickness, temperature profiles, and for the components of the velocity field will be the focus of the discussion. In order to produce illustrative results for the system, a reference fluid must be identified and, in this case, the physical properties of water have been chosen for such a purpose. This is necessary to calculate reasonable values of dimensionless numbers, Reynolds and Grashof, required by Eqs. (25a) and (25b). In addition, these equations also required a value for the source generation term, ϕ^2, for their solution. This particular requirement gives the opportunity to study the role of the heating effect being analyzed in this work. In consequence, a valid range of physical values must be defined. Positive values of ϕ^2 indicate heat generation, and therefore, the following range has been chosen

$$0 \le \phi^2 \le 5. \qquad (26)$$

From the previous range and for analysis purposes, four ϕ^2 values have been selected as $\phi^2 = 0$, $\phi^2 = 1.5$, $\phi^2 = 3.0$, and $\phi^2 = 5.0$. The $\phi^2 = 0$ has been included as a reference value for the case of no Joule heating effect. On the other hand, the $\phi^2 = 5.0$ has been selected as a maximum considering that such a value produces an increase in the slope of the boundary layer near the origin of four times (300%) the values for the case of no Joule heating effect. The other two have been selected within the range. With the set of valid ϕ^2, temperature profiles, boundary layer thickness, and velocity profiles have been illustrated and they are presented next.

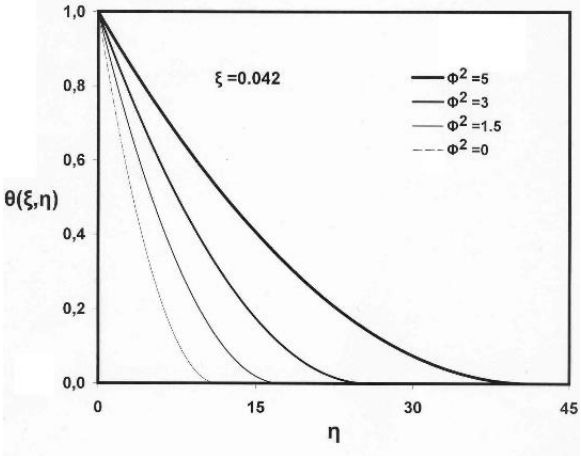

Figure 2: Dimensionless temperature profiles (inside the boundary layer) for various values of the heat generation source term and for the η-direction (ξ =0.042).

Figure 2 shows a parametric representation of the influence of Joule heating generation on temperature profiles inside the boundary layer domain. Furthermore, the figure shows that the range of acceptable ϕ^2 values produces a family of exponential decay type curves. In particular, this figure illustrates temperature variation as a function of the transversal direction of the boundary layer (η) for a given value of axial direction, (ξ=0.042). For all given values of ϕ^2 the temperature at the surface of the electrode remain at the value of θ =1. Specifically, for a value of ϕ^2 equal to 5.0 the temperature has a variation between the values of θ = 1, at the electrode surface, and a value of θ = 0, i.e. fluid temperature, at η approximately equal to 40. A decrease in ϕ^2 values from 5.0 to 3 yields a reduction on the η value from 40 to 25 in order to reach the same fluid temperature. From a cross sectional analysis on η=10, the figure predicts that this 40% reduction in ϕ^2 value will cause a reduction of approximately 35% in temperature values. Further reduction in ϕ^2 values from 3.0 to 1.5 produces a decrease on the η value from 25 to 17 as to both obtain the fluid temperature. A similar trend, as the one previously reported, is observed on this 50% reduction in ϕ^2 that will cause a reduction of approximately 52% in temperature values. Therefore, the system temperature shows high sensitivity to the Joule heating effect.

Figure 3 displays temperature variation along the axial coordinate ξ for a given position of η (η=3). A single identifiable trend along the axial coordinate, ξ, is clearly observed. For each value of ϕ^2 chosen within its range the temperature profiles describe an inverse exponential function of different amplitudes, respectively. The higher the value of ϕ^2 the wider is the amplitude of the curve. Additionally, near the electrode region (ξ < 0.03, approximately) steep variations in temperature values are developed in all cases to reach different plateau values beyond ξ = 0.04, approximately, with an incipient transition in between. This just described temperature behavior has been also identified elsewhere on an analytical solution approach of this differential boundary layer model.

Figure 4 illustrates the effect of Joule heating on the dimensionless boundary layer thickness along the axial coordinate, ξ, for different values of the source generation term, ϕ^2. In terms of the same ϕ^2 values, there are two trends observed: the first is described by ϕ^2 approximately less than 3 and the second by greater values. In the first case the boundary layer thickness follows a similar qualitative behavior as the temperature described in Fig. 3, above. In other words, a single identifiable region, described as an inverse exponential function, is also observed in the variation of the dimensionless boundary layer thickness, δ^+, for low ϕ^2 values. In addition, steady slope variations of δ^+ are observed for ξ values approximately greater than 0.01 while a steeper variation of δ^+ develops near the electrode origin, this is for ξ values smaller than 0.01. Finally, for the second trend, at high ϕ^2 values, the general variation in the boundary layer thickness, δ^+, is a straight line where the exponential type of curve trend is completely missing.

Figure 5 shows the development of different dimensionless axial velocity profiles, induced by Joule heating

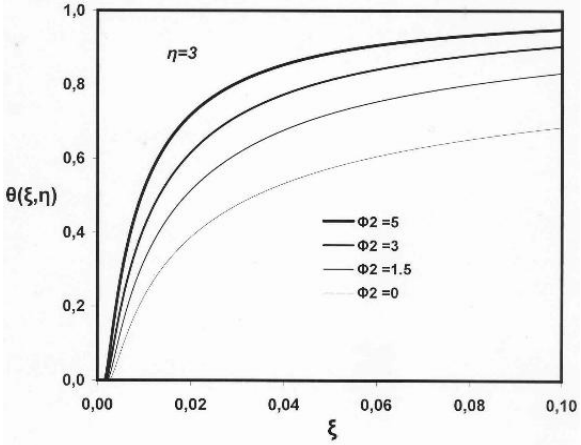

Figure 3: Dimensionless temperature profiles (inside the boundary layer) for various values of the heat generation source term and for the ξ-direction (η =3).

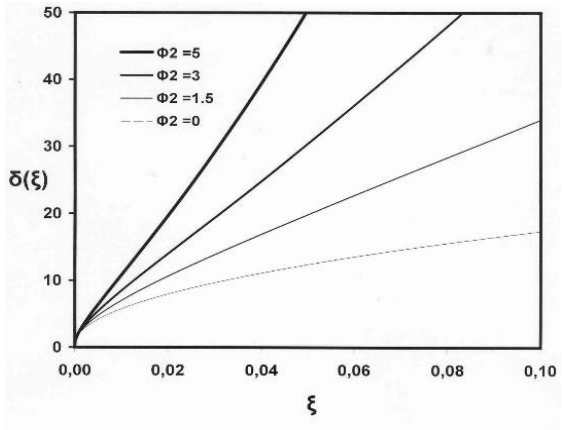

Figure 4: Dimensionless boundary layer thickness for different values of the heat generation source term.

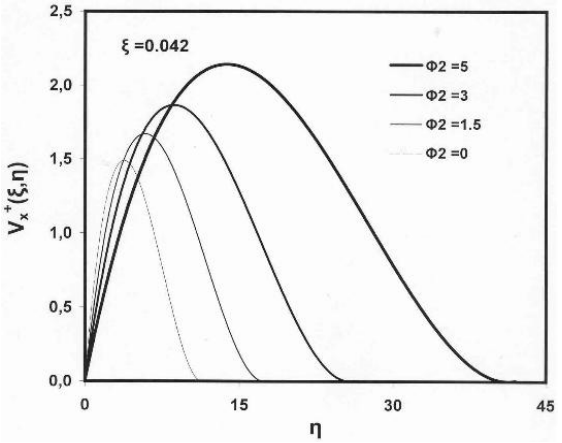

Figure 5: Dimensionless total velocity profiles showing the effect of the heat generation inside the boundary layer for the η-direction (ξ =0.042).

generation, along the transversal axes, η, inside the boundary layer domain, for a given position in the axial direction, (ξ=0.042). Additionally, the figure exhibits for all the selected ϕ^2 values a family of curves that mimic a parabolic type of curve (as proposed by the Von Karman model) with a slowly decaying end at the region far away from the electrode. On the other hand, for all selected ϕ^2 values the dimensionless axial velocities at the surface of the electrode stay at the value of $v_x^+ = 0$. This is in agreement with the non-slip boundary condition of zero velocity at the electrode surface. Particularly, for a value of ϕ^2 equal to 5.0 the dimensionless axial velocity has a maximum of $v_x^+ = 2.14$ at approximately η=14, this is 1.4 times the value that corresponds to the η point for the no Joule heating effect (η=4) and it represents a 44% increase in velocity from the no heating effect case. The same analysis with φ^2 value of 3.0 generates a maximum velocity of $v_x^+ = 1.86$ at η=9, this is a 25% increase in the velocity from the maximum for the no Joule heating effect case. For the case of ϕ^2 equal to 1.5, the value of η at the maximum velocity is 50% larger than the case of no Joule heating effect and the point represents an increase of 12% on the velocity magnitude. From this analysis, clearly the sensitivity of the system to the Joule heating effect is reasonably high and practical cases without accounting for Joule heating generation will occur in a significant error in velocity predictions.

Figure 6 depicts dimensionless axial velocity profiles variation along the axial coordinate ξ for a given position of η (η=3). The general trend indicates that higher ϕ^2 values, first, increase velocity profiles toward individual maxima and, later, reduce the magnitude of velocity for any ξ value beyond these maxima. On the other hand, the $\phi^2 = 0$ value, no heat generation case, describes a parabolic type of curve reaching a maximum velocity without decay beyond this point. In particular,

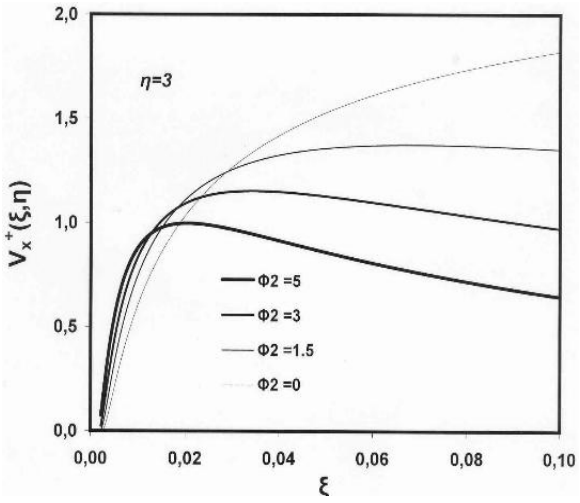

Figure 6: Dimensionless total velocity profiles showing the effect of the heat generation inside the boundary layer for the ξ-direction (η =3).

velocity profiles affected by heat generation are greater than the expected without Joule heating effect along the axial coordinate ξ until they reach a point of equality. Beyond this point all the velocity profiles are smaller than the corresponding without heating effect. A cross sectional analysis of the axial velocity on $\xi = 0.04$ for ϕ^2 =1.5, $\phi^2 = 3.0$, and $\phi^2 = 5.0$ values yields velocities decay of 7%, 19%, and 36% respectively with respect to the value for the case of no Joule heating generation.

IV. SUMMARY AND CONCLUDING REMARKS

An analysis has been performed for natural convection boundary layer flows with Joule heating generation. These flows are of relevance in applications such as in electrokinetic remediation and electrophoretic separation processes. The integral approximation approach originally proposed by Von Karman was used to invert the boundary layer model in order to derive a simpler, two first order, differential equation model. The addition of the Joule heating generation term and the changing of the Dirichlet boundary conditions (to wall condition instead of fluid) lead to important modifications whose solution is not trivial. The assumption that the heat generation follows a similarity type of function (Oyanader, 2004) does not yield an analytical solution and therefore a numerical solution is required. In other words, the source generation term, ϕ^2, shows a constant value along ξ, the axial- coordinate of the system which is not obtained when a similarity solution is assumed (see Oyanader *et al*., 2007). As part of the solution approach, dimensionless ordinary integro-differential equations have been derived. These equations have been solved using dimensionless temperature and velocity profiles that are functions of ξ and η, dimensionless coordinates. The numerical solution has been illustrated by using the physical properties of aqueous solutions. The effect of heat generation on temperature and velocity profiles, as well as on the boundary layer thickness, has been discussed. A major finding is that Joule heating generation affects considerably the value of the temperature, the boundary layer thickness and both velocities components of the hydrodynamic field inside the boundary layer. These findings could be used advantageously in processes such as in electrokinetic remediation and/or electrophoretic separation depending upon the experimental conditions and transport properties of the system. For example, the increase in the velocity magnitudes may lead to important mixing conditions near the electrode surface that for relatively small cells will decrease the treatment efficiency of the process. On the other hand, the increase in the velocity magnitude may, actually helps to transport species in the direction of the flow and, therefore, increase the overall efficiency of the process for larger cells. The results here should be taken as basic trends since, for example, electro-osmosis flows have been neglected. Their presence may, actually, modify some of the conclusions reported here. This analysis, however, will be presented elsewhere.

ACKNOWLEDGEMENTS

The support provided by Universidad Católica de Norte, Chile, and the Fulbright Commission to the doctoral work of Mario A. Oyanader is specially acknowledged.

REFERENCES

Acar, Y.B., R. Gale, A. Alshawabkeh, R. Marks, S. Puppala, M. Bricka and R. Parker. "Electrokinetic Remediation: Basics and Technology Status," *Journal of Hazardous Materials*, **40**, 117-137 (1995).

Bird, R.B; W. Stewart and E N. Lightfoot, *Transport Phenomena*, John Wiley and Sons, Inc., New York. (1960).

Chilingar, G.V., W.W. Loo, L.F. Khilyuk and S.A. Katz "Electrobioremediation of soils contaminated with hydrocarbons and metal: progress report," *Energy Sources*, **19**, 129-146 (1997).

Erdmann, L., M.A. Oyanader and P. Arce, "Effect Of the Joule Heating and Of the Material Voids on Free-Convective Transport In Porous Or Fibrous Media With Applied Electrical Fields," *Electrophoresis*, **26**, 2867-2877 (2005).

Ho, S.V., C. Athmer, P. Sheridan and A. Shapiro, "Scale up Aspect of Lasagna process for In Situ Soil Decontamination," *Journal of Hazardous Materials,* **55**, 221-237 (1997).

Kreyzing, E., *Advanced Engineering Mathematics*, John Wiley and Sons, Inc., New York (1999).

Langeman, R., "Electroreclamation: Application in the Netherlands," *Environmental Science Technology*, **27**, 2648-2650 (1993).

Masliyah, J., *Electrokinetic Transport Phenomena*, AOSTRA Technical Publication Series No. 12, Alberta, Canada (1994).

Oyanader, M., P. Arce and A. Dzurik, "Avoiding Pitfalls in Electrokinetic Remediation: Robust Design and Operation Criteria Based on First Principles for Maximizing Performance in a Rectangular Geometry," *Electrophoresis*, **24**, 3457-3466 (2003).

Oyanader, M.A., "Physicochemical Hydrodynamics of Electrokinetics in Soil Remediation," Ph.D. Thesis, Florida State University (2004).

Oyanader, M., P. Arce and A. Dzurik, "Design Criteria for Soil Cleaning Operations in Electrokinetic Remediation. Hydrodynamic Aspects in an Annular Geometry," *I&ECh Research*, **44**, 6200-6411 (2005a).

Oyanader, M., P. Arce and A. Dzurik, "Design Criteria for Soil Cleanning Operations in Electrokinetic Remediation. Hydrodynamic Aspects in a Cylindrical Geometry," *Electrophoresis*, **26**, 2878-2887. (2005b).

Squire, H.B., "*Modern Developments of Fluid Dynamics*," Oxford University Press, London, 641 (1938).

Turnbull, R.J., "Free Convection from Heated Vertical Plate in a Direct-Current Electrical Filed," *Physics of Fluids*, **12**, 2255 (1969).

Virkutyte, J., M. Sillanpaa and P. Latostenmaa, "Electrokinetic Soil Remediation – Critical Overview," *The Science of the Total Environment*, **289**, 97-121 (2002).

Whitaker, S., *Introduction to Fluid Mechanics*, Krieger Publishing Company, Malabar, Florida, 3rd Ed. (1991).

Gebhart, B., Y. Jaluria, R. Mahajan and B. Sammakia, *Buoyancy-Induced Flows and Transport*, Hemisphere Publishing Company, New York (1988).

Yeung, A., C. Hhsu and R.M. Menon, "Physicochemical Soil-Contaminant Interaction During Electrokinetic Extraction," *Journal of Hazardous Materials,* **55**, 221-237 (1997).

Received: February 17, 2007.
Accepted: September 5, 2007.
Recommended by Subject Editor: Walter Ambrosini